Oxide characterization of Fe-Cr-Si alloys formed in high-temperature water

Kien Trung Le[a], Jaheon Kim[a], Chi Bum Bahn[a]*
[a]*School of Mechanical Engineering, Pusan National University, Busan, Republic of Korea*
[*]*Corresponding author: bahn@pusan.ac.kr*
Keywords : Accident Tolerant Fuel, Fe-Cr-Si alloy, corrosion, dual protective layer

1. Introduction

Zirconium alloy cladding exhibits excellent corrosion resistance under normal operating conditions; however, it undergoes severe oxidation in high-temperature steam, generating hydrogen that can lead to explosions, as exemplified by the 2011 Fukushima nuclear accident [1]. Therefore, the development of accident-tolerant fuel (ATF) cladding materials to replace zirconium alloys is essential. Several promising candidates have been proposed, including FeCrAl, SiC/SiC composites, and Fe-Cr-Si alloys. While FeCrAl and SiC/SiC have been extensively investigated, studies on Fe-Cr-Si alloys remain limited, particularly regarding their long-term corrosion behavior in simulated PWR primary water [2,3,4]. To address this gap, the present study investigates the long-term corrosion behavior of Fe16Cr2Si and Fe20Cr2Si exposed to simulated PWR primary water, with Fe20Cr employed as a Si-free reference to isolate the effect of Si addition.

2. Methods

Three model alloys, Fe20Cr, Fe16Cr2Si, and Fe20Cr2Si (in wt%), were prepared as 10 × 10 × 2 mm coupons and polished up to a 0.06 μm surface finish. The specimens were then ultrasonically cleaned in acetone, ethyl alcohol, and deionized water for 10 min each, dried, and weighed. Long-term corrosion tests were conducted in a static autoclave made of INCOLOY 800H with a volume of 2100 mL. The test pressure and temperature were 19 MPa and 360 °C, respectively. The test solution was prepared by dissolving 1200 ppm B and 2 ppm Li in deionized water and was deaerated with Ar gas prior to testing. Corrosion tests were performed for exposure durations of 250, 500, 1000, and 2000 h. After each interval, the specimens were removed, rinsed, dried, and reweighed, and the test solution was completely replaced before the test was resumed.

After the corrosion tests, the oxide surfaces were examined by scanning electron microscopy (SEM). X-ray diffraction (XRD) was used to identify the phases present in the oxide layer, and X-ray photoelectron spectroscopy (XPS) was employed to analyze the oxide layer composition and chemical states.

3. Results and Discussion

3.1 Comparison of mass change

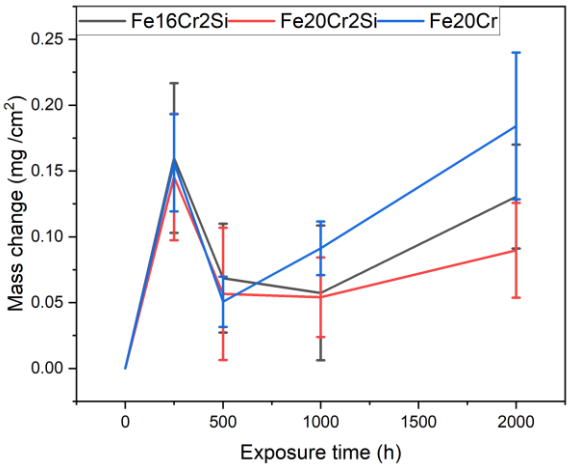


Figure 1. Comparison of mass change (mg/cm^2) of Fe-Cr-Si alloys with different exposure times.

All alloys showed a sharp mass increase at 250 h, followed by a significant drop at 500 h, indicating that oxide dissolution outweighed oxide growth during this stage; the complete replacement of the test solution after each interval may have promoted dissolution by resetting the degree of saturation. From 1000 h onwards, the three alloys began to diverge according to their composition. After 2000 h, Fe20Cr2Si exhibited the lowest mass gain while Fe20Cr showed the highest, confirming the critical role of Si in long-term corrosion resistance. These results suggest that the combination of high Cr and Si content provides the most effective protection in deaerated PWR-chemistry water over extended exposure periods.

3.2 Surface oxide characterization

As shown in the Figure. 2, most of the XRD patterns show that the oxide products formed on the specimen surfaces after exposure were Fe_3O_4 and $FeCr_2O_4$. The absence of any Cr- or Si-based oxides can be attributed to their layers being too thin to be detected by XRD [2]. In addition, distinguishing between the Fe_3O_4 and $FeCr_2O_4$ peaks, as well as between the Fe and Cr peaks, is difficult because their positions are very close to one another.

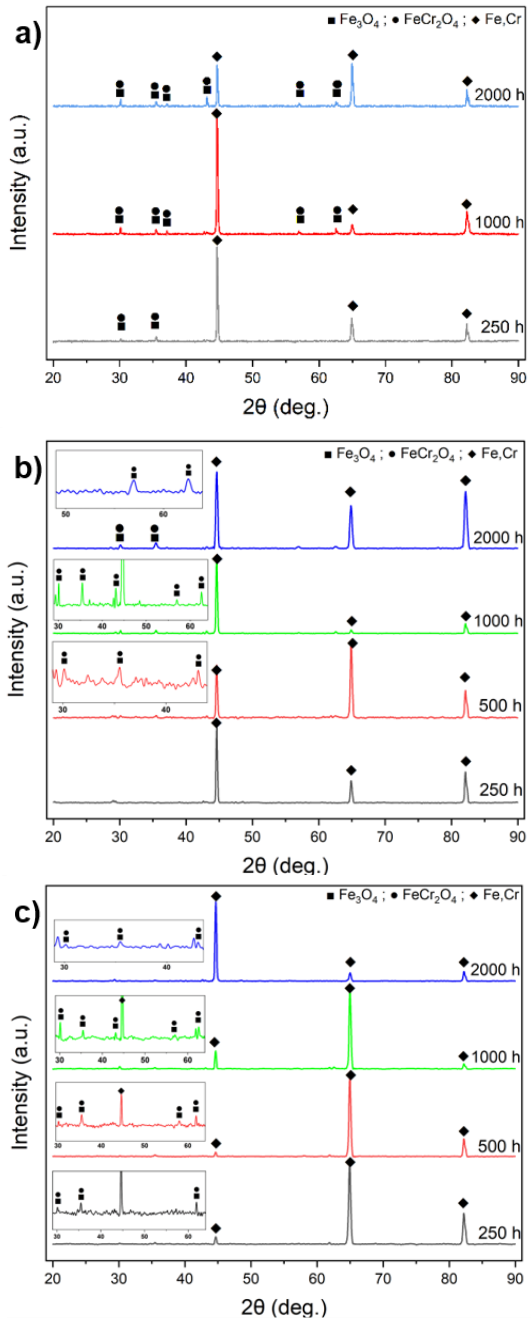


Figure 2. XRD pattern of. (a) Fe16Cr2Si, (b) Fe20Cr, and (c) Fe20Cr2Si

3.3 Oxide morphology

Figure. 3 shows the surface morphologies of the three alloys after 2000 h of exposure. Fe20Cr2Si exhibited the lowest density of surface oxide particles, followed by Fe20Cr and Fe16Cr2Si. Since these faceted crystallites are precipitates formed from the solution, their surface density does not necessarily follow the mass-change ranking in Figure. 1.

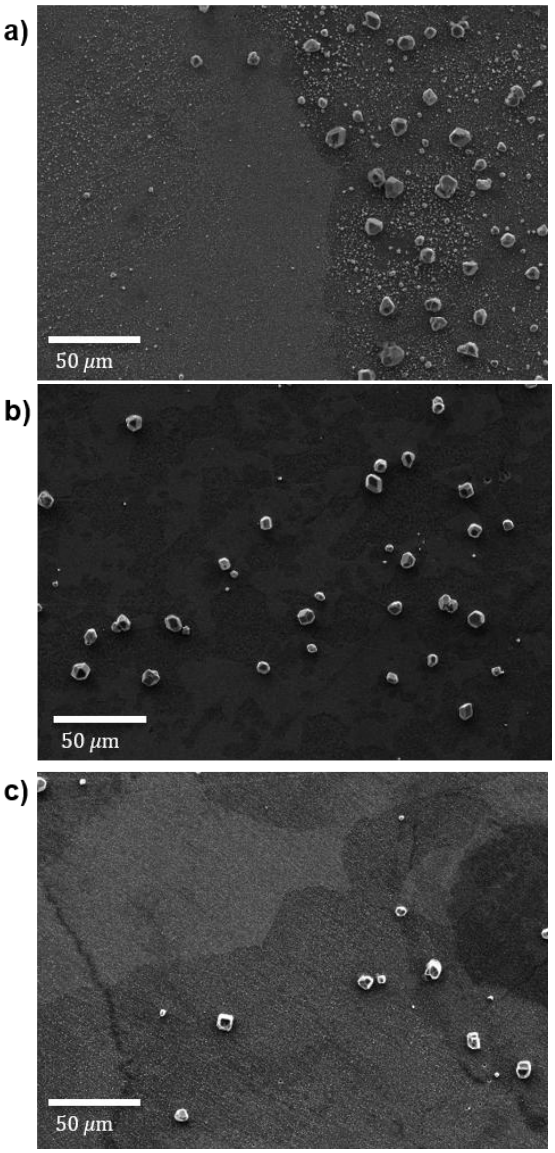


Figure 3. SEM surface morphologies after 2000 h of exposure: a) Fe16Cr2Si, b) Fe20Cr, c) Fe20Cr2Si.

3.4 Oxide layer

Figure. 4 shows the XPS depth profiles of the three specimens after 2000 h of exposure. The sputtering time required to reach the oxide/metal interface increased in the order Fe16Cr2Si < Fe20Cr2Si < Fe20Cr, indicating that both Si-containing alloys formed thinner oxides than the Si-free reference. The interface was identified using two criteria: the metallic signals approaching the nominal bulk compositions, and the O 1s signal falling below 5 wt%. Since the sputtering conditions were identical for all specimens, the sputtering time can be regarded as a relative measure of oxide thickness.

The two Si-containing alloys also differed in the internal Cr distribution. In Fe20Cr2Si, Cr increased from the surface to a distinct maximum within the oxide, indicating a Cr-enriched region, whereas in Fe16Cr2Si Cr was enriched only at the outermost surface and

decreased monotonically with depth. The Cr-enriched region in Fe16Cr2Si was therefore less pronounced than in Fe20Cr2Si, consistent with its lower Cr content.

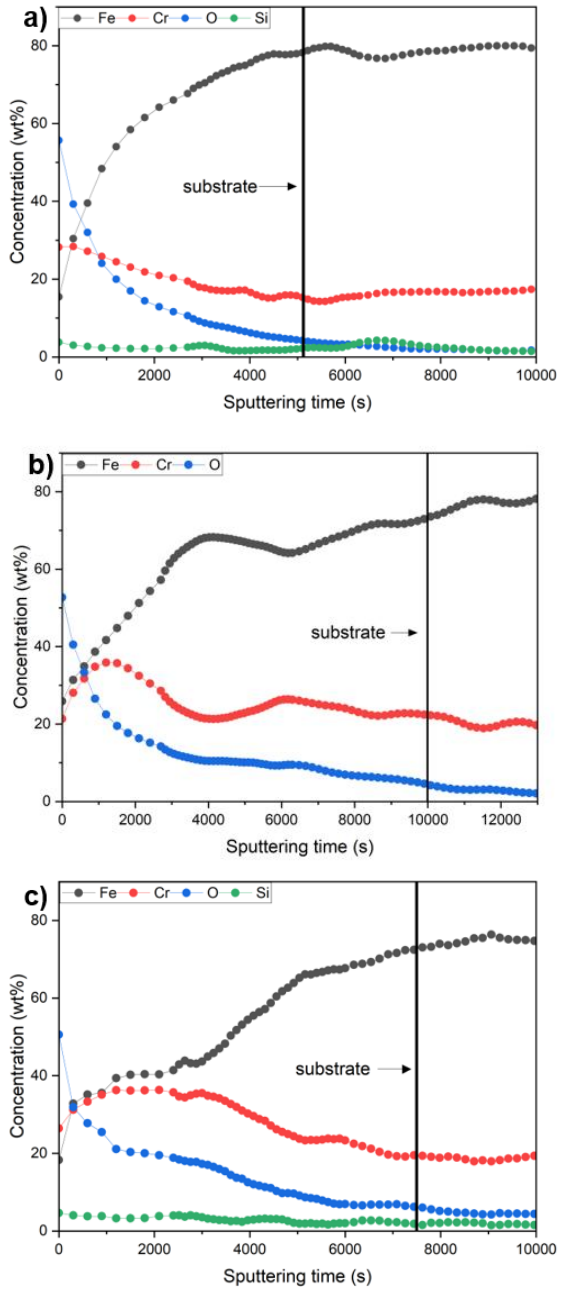


Figure 4. XPS depth profiles of (a) Fe16Cr2Si, (b) Fe20Cr, and (c) Fe20Cr2Si after 2000 h of exposure.

As shown in Figure 5, Cr^{3+} and Si^{4+} species were detected near the oxide/metal interface of Fe20Cr2Si, confirming the formation of Cr_2O_3 and SiO_2 in the inner oxide. Although Fe16Cr2Si developed the thinnest oxide, Fe20Cr2Si exhibited the lowest mass gain after 2000 h. This apparent discrepancy suggests that corrosion resistance is governed by the composition and internal distribution of the oxide rather than by its total thickness alone, with the Cr_2O_3- and SiO_2-containing inner region of Fe20Cr2Si appearing more effective in limiting further oxidation. Fe20Cr showed both the longest sputtering time and the highest mass gain, indicating that 20 wt% Cr alone is inadequate under these conditions and that the additional formation of a Si-rich oxide is required for improved corrosion resistance.

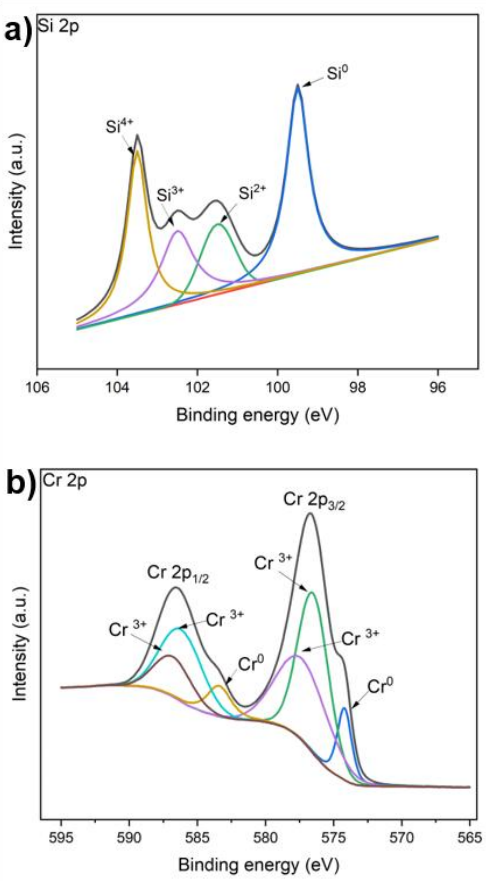


Figure 5. (a) Si 2p and (b) Cr 2p spectra acquired near the oxide/metal interface of Fe20Cr2Si after 2000 h of exposure in simulated PWR primary water.

4. Conclusions

The corrosion behavior of Fe20Cr, Fe16Cr2Si, and Fe20Cr2Si was investigated in deaerated PWR-chemistry water for up to 2000 h. Both Si-containing alloys outperformed the Si-free Fe20Cr reference in mass gain and oxide thickness, confirming that Si addition is the dominant factor governing long-term corrosion resistance. Among them, Fe20Cr2Si showed the lowest mass gain while Fe16Cr2Si developed the thinnest oxide, indicating that oxide composition rather than thickness governs the difference: Fe20Cr2Si formed a Cr-enriched region within the oxide, whereas in Fe16Cr2Si the Cr enrichment was confined to the outer surface. The detection of Cr^{3+} and Si^{4+} near the oxide/metal interface confirms the formation of Cr_2O_3 and SiO_2, which act as the protective constituents of the inner oxide. Fe-Cr-Si alloys, particularly Fe20Cr2Si, therefore appear promising as ATF cladding candidates with respect to normal-operation corrosion resistance.

REFERENCES

[1] R. Yoshioka, K. Iino, TECHNICAL REPORT: FUKUSHIMA ACCIDENT SUMMARY (AUG. 19, 2011), 2011.
[2] R. Qiang, A. Leong, J. Zhang, M. P. Short, Corrosion behavior of Fe-Cr-Si alloys in simulated PWR primary water environment, Journal of Nuclear Materials, 526 (2019) 151735.
[3] A. Leonga, Q. Yanga, S. W. McAlpineb, M. P. Shortb, J. Zhang, Oxidation behavior of Fe-Cr-2Si alloys in high temperature steam, Corrosion Science, 179(2021)109114.
[4] J. Moon, S. Kim, W. D. Park, T. Y. Kim, S. W. McAlpine, M. P. Short, J. H. Kim, C. B. Bahn, Initial oxidation behavior of Fe-Cr-Si alloys in 1200°C steam, Journal of Nuclear Materials. 513 (2019) 297-308.